Thymic dendritic cell-derived IL-27p28 promotes the establishment of functional bias against IFN-γ production in newly generated CD4^{+} T cells through STAT1-related epigenetic mechanisms

Jie Zhang[1], Hui Tang[1], Haoming Wu[1], Xuewen Pang[1], Rong Jin[1*], Yu Zhang[1,2*]

[1] Department of Immunology, School of Basic Medical Sciences, NHC Key Laboratory of Medical Immunology, Medicine Innovation Center for Fundamental Research on Major Immunology-related Diseases, Peking University, Beijing, China

2 Institute of Life Sciences, Jinzhou Medical University, Jinzhou, Liaoning Province, China

Corresponding Author

Yu Zhang, zhangyu007@bjmu.edu.cn

Rong Jin, jinrong@bjmu.edu.cn

Keywords: IL-27p28, single positive thymocyte, Th2 bias, IFN-γ, autoimmune disease

Abstract

The newly generated CD4 single-positive (SP) T lymphocytes are featured by enhanced IL-4 but repressed IFN-γ production. The mechanisms underlying this functional bias remain elusive. Previous studies have reported that $CD4^+$ T cells from mice harboring DC-specific deletion of IL-27p28 display an increased capacity of IFN-γ production upon TCR stimulation. Here we demonstrated that similarly altered functionality occurred in CD4SP thymocytes, recent thymic emigrants (RTEs), as well as naive T cells from either *Cd11c-p28*$^{f/f}$ mice or mice deficient in the α subunit of IL-27 receptor. Therefore, DC-derived IL-27p28-triggered, IL-27Rα-mediated signal is critically involved in the establishment of functional bias against IFN-γ production during their development in the thymus. Epigenetic analyses indicated reduced DNA methylation of the *Ifng* locus and increased trimethylation of H3K4 at both *Ifng* and *Tbx21* loci in CD4SP thymocytes from *Cd11c-p28*$^{f/f}$ mice. Transcriptome profiling demonstrated that *Il27p28* ablation resulted in the coordinated up-regulation of STAT1-activated genes. Concurrently, STAT1 was found to be constitutively activated. Moreover, we observed increased accumulation of STAT1 at the *Ifng* and *Tbx21* loci and a strong correlation between STAT1 binding and H3K4me3 modification of these loci. Of note, *Il27p28* deficiency exacerbated the autoimmune phenotype of *Aire*$^{-/-}$ mice. Collectively, this study reveals a novel mechanism underlying the functional bias of newly generated $CD4^+$ T cells and the potential relevance of such a bias in autoimmunity.

41 Graphical abstract

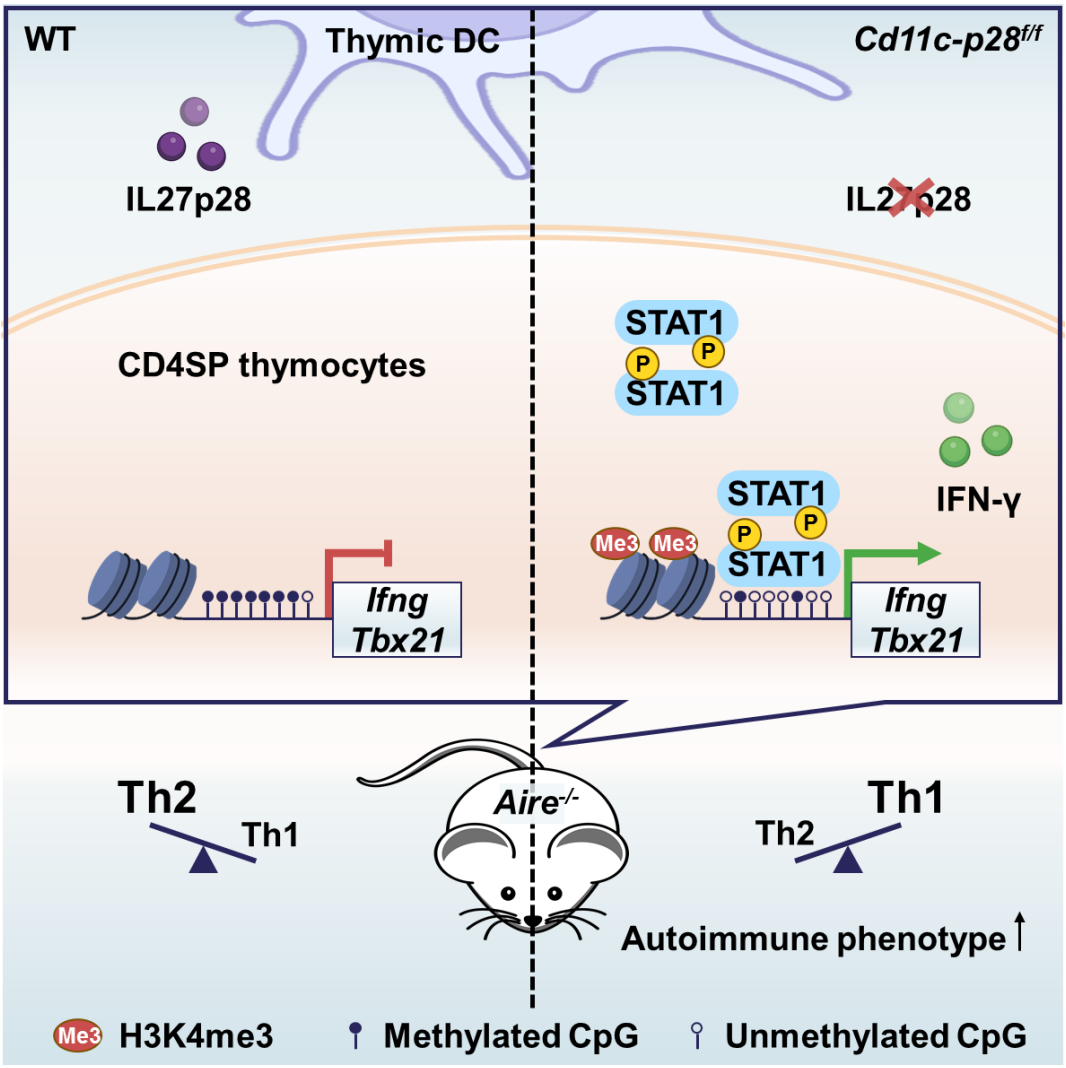

42

Introduction

The thymus plays a crucial role in the phenotypic development and functional maturation of T cells. After positive and negative selection, T cell progenitors become CD4 or CD8 single positive (CD4SP or CD8SP) thymocytes that are self-tolerant. These SP thymocytes then emigrate to the periphery, known as recent thymic emigrants (RTEs), and 2-3 weeks later, RTEs develop into mature naive T cells (Ashby & Hogquist, 2023). Upon activation, CD4SP thymocytes and RTEs exhibit a reduced proliferation capacity and decreased production of interleukin-2 (IL-2), interferon-γ (IFN-γ), and tumor necrosis factor α (TNF-α) compared to mature naive T cells. However, they show increased secretion of IL-4, which is known as T helper (Th) 2 bias in immature T cells (Hendricks & Fink, 2011). This Th2 bias in CD4SP thymocytes and RTEs is thought to assist newly emigrated self-reactive T cells to respond appropriately to self-antigens (Fink & Hendricks, 2011). Furthermore, the low level of IFN-γ production in RTEs renders them more prone to becoming regulatory T cells, which also helps to prevent the induction of autoimmune diseases (Bhaumik et al., 2013). The low level of DNA methylation at the *Il4* locus and reduced expression of *Dnmts* contribute to the Th2 bias in CD4SP thymocytes and RTEs (Berkley, Hendricks, Simmons, & Fink, 2013). However, the mechanism behind repressed IFN-γ expression in favor of the Th2 bias in these immature T cells is elusive.

The heterodimeric cytokine IL-27 is composed of IL-27p28 and Epstein-Barr virus-induced gene 3 (EBI3), which signals through the IL-27R consisting of the IL-27Rα (also named WSX-1, TCCR) and the gp130 subunits. Elevated levels of IL-27

are associated with the pathogenesis of autoimmune diseases such as ankylosing spondylitis (AS) (Lin et al., 2015), Behcet's disease (BD) (Shen, Xia, & Lu, 2013), and experimental arthritis (Cao, Doodes, Glant, & Finnegan, 2008). The IL-27-regulated differentiation and function of peripheral $CD4^+$ T cells subsets Th1, Th17 and Treg have been proposed as an explanation for the pathogenesis of autoimmune disease (Mei et al., 2021), however, conflicting reports have been demonstrated in different settings. For example, it is consistent that IL-27 inhibits Th17 differentiation and function *in vitro* and *in vivo* in *Il27p28*$^{-/-}$ and *Ebi3*$^{-/-}$ experimental autoimmune encephalomyelitis (EAE) mice models (Diveu et al., 2009; Kim et al., 2019; Liu et al., 2012). Although IL-27 inhibits Treg differentiation *in vitro* (Huber et al., 2008; Neufert et al., 2007), and *Ebi3*$^{-/-}$ EAE models show increased numbers and suppressive functions of Tregs (Liu et al., 2012), Tregs in *Il27ra*$^{-/-}$ and Treg-specific *Il27ra*$^{-/-}$ mice loss the suppressive function (Kim et al., 2019; Nguyen et al., 2019; Y. J. Park et al., 2019). Furthermore, IL-27 was initially found to promote Th1 differentiation of naive $CD4^+$ T cells under physiological conditions (Pflanz et al., 2002). However, naive $CD4^+$ T cells derived from *Ebi3*$^{-/-}$ and *Il27p28*$^{-/-}$ mice exhibit increased production of IFN-γ. In addition, the absence of *Il27ra*$^{-/-}$ promotes pathological Th1 accumulation following *Trypanosoma cruzi* infection (Hamano et al., 2003). A subsequent study demonstrates that both the absence and overexpression of IL-27p28 lead to increased susceptibility to *T. gondii* infection, highlighting the role of IL-27p28 as an independent negative regulator of IFN-γ production in T cells (J. Park et al., 2019; Villarino et al., 2003). Notably, deficiency in gp130 does not alter IFN-γ production in $CD4^+$ T cells in a virus-infection

model (Harker, Wong, Dolgoter, & Zuniga, 2015). These results indicate the intricate functionality of each subunit of IL-27 and IL-27R in peripheral $CD4^+$ T cells, which complicates the interpretation of the autoimmune phenotype in deficient mice.

The structural analysis of IL-27 has demonstrated that IL-27p28, serving as a central subunit, possesses the ability to bind with EBI3, as well as the receptor subunits IL-27Rα (Caveney, Glassman, Jude, Tsutsumi, & Garcia, 2022). Previous studies have reported IL-27p28 as an independent antagonist of gp130-mediated signaling (Stumhofer et al., 2010). In a ConA-induced liver damage model, $CD4^+$ T cells from mice with dendritic cell (DC)-specific deletion of p28 (*Cd11c-p28*$^{f/f}$ mice) exhibit a propensity for rapid and robust production of IFN-γ upon activation. This observation is attributed to the absence of IL-27p28 in the thymic environment of these mice (Zhang et al., 2013). These findings raise the intriguing possibility that thymic DC-derived IL-27p28 may contribute to shaping the Th1/Th2 balance of newly generated CD4SP thymocytes.

In this paper, we have demonstrated that DC-derived IL-27p28 plays a crucial role in maintaining the Th2 bias of CD4SP thymocytes. Our findings suggest that IL-27p28 regulates the DNA methylation status and histone modifications in the transcription regulatory regions of *Ifng* and *Tbx21* genes. These epigenetic modifications were further modulated by the low level of basal and phosphorylated signal transducer and activator of transcription 1 (STAT1) protein. Furthermore, we observed that the disruption of Th2 bias in CD4SP thymocytes due to IL-27p28 deficiency exacerbated autoimmune diseases in *Aire*$^{-/-}$ mice. Our results provide insights into the molecular

109 mechanisms underlying the regulation of Th2 bias by DC-derived IL-27p28 and its

110 potential role in autoimmune diseases.

Results

1. DC-specific deletion of IL-27p28 endows the newly generated CD4$^+$ T cells with inherently enhanced capacity of IFN-γ production

Although IL-27 is widely reported to promote peripheral Th1 differentiation *in vitro*, CD4$^+$ T cells from *Cd11c-p28$^{f/f}$* mice exhibit enhanced IFN-γ production, a capacity seemingly acquired in their development in the thymus (Zhang et al., 2013). To investigate the possibility that thymic DC-derived IL-27 shapes the functionality of newly generated CD4$^+$ T cells, CD4SP thymocytes, CD4$^+$ RTEs, and CD4$^+$ naive T cells were purified from *Cd11c-p28$^{f/f}$* (cKO) mice and their wild-type (WT) littermates harboring a Rag2-GFP transgene, which allows easy tracking of newly generated thymocytes and RTEs (Ashby & Hogquist, 2023). The purified cells were then compared for cytokine expression in response to anti-CD3 and anti-CD28 stimulation under non-polarizing conditions. As expected, CD4$^+$ naive T cells from cKO mice exhibited a significantly higher level of *Ifng* mRNA expression compared to WT cells (Figure 1A). Intracellular staining (Figure 1B) and ELISA assay of the culture supernatant (Figure 1C) confirmed enhanced IFN-γ production at the protein level. Notably, this difference was already detectable at the SP thymocyte stage, indicating that it is developmentally regulated. Another prominent feature of CD4SP thymocytes is the hyperproduction of Th2 cytokines (Fink & Hendricks, 2011; Makar et al., 2003). Despite the profound impact of IL-27p28 deficiency on IFN-γ production, we observed no significant difference in IL-4 expression between cKO and WT T cells (Figure 1A and C). Moreover, there was no significant difference in the expression of IL-2 and

133 TNF-α between cKO and WT T cells (Figure 1A and Figure 1-figure supplement 1).
134 These results suggest that DC-specific deletion of IL-27p28 specifically enhances IFN-
135 γ production in newly generated T cells without affecting Th2 cytokines.

136 Next, we investigated the expression of T-box transcription factor (T-bet) and
137 GATA3, which are the master regulators of Th1 and Th2 differentiation, respectively
138 (Fang, Healy, & Zhu, 2022). The differential impact of IL-27p28 deficiency on IFN-γ
139 and IL-4 production was accompanied by an increase in Tbx21 expression but no
140 significant alteration in Gata3 expression (Figure 1D). Western blotting and flow
141 cytometry confirmed the upregulation of T-bet protein expression (Figure 1E, F).
142 Furthermore, we extended our analyses onto $CD4^+$ T cells at steady state or under
143 polarizing conditions. Higher basal levels of *Ifng* and *Tbx21* transcripts were detected
144 in CD4SP thymocytes and naive T cells from cKO mice than the counterparts from WT
145 mice even without stimulation (Figure 1G), indicating the constitutive activation of
146 these loci. When cultured under polarizing conditions, these cells were effectively
147 induced to differentiate into Th1, Th2, Th17 and Treg lineages. In contrast to the
148 previous report of different differentiation potentials of RTEs versus naive T cells
149 (Hendricks & Fink, 2011), CD4SP thymocytes, RTEs and naive T cells showed similar
150 capacity to differentiate into effector cells. Moreover, cKO and WT cells were equally
151 positioned for the differentiation (Figure 1-figure supplement 2A-F), suggesting that
152 IL-27p28 deficiency does not affect effector cell differentiation under optimal
153 conditions. Moreover, the frequency of IFN-γ-, and granzyme B-producing $CD8^+$ T
154 cells under Th0 conditions was comparable between cKO and WT T cells (Figure 1-

figure supplement 2G). Taken together, these data support that IL-27p28 is actively involved in the functional maturation of developing CD4SP thymocytes, biasing them away from the Th1 lineage.

2. *Il27ra*-deficient CD4$^+$ T cells are similarly predisposed for potent IFN-γ production

Apart from acting as a subunit of IL-27, IL-27p28 have been reported to possess activities independent of IL-27, by acting on its own or coupling with other proteins, such as IL-Y (p28/p40, binding to IL-27Rα/IL-12Rβ1 to activate STAT3) (Flores et al., 2015) and CLY (p28/CLF, binding to gp130/IL-6Rα to activate STAT1 and STAT3) (Tormo et al., 2013). To ascertain whether the phenotype in the *Cd11c-p28$^{f/f}$* mice results from defective IL-27Rα signaling, we investigated the functional characters of T lineage cells in mice deficient in *Il27ra*. Reminiscent to what was observed in *Il27p28*-deficient mice, increased expression of *Ifng* and *Tbx21* were detected in *Il27ra$^{-/-}$* CD4SP thymocytes and naive CD4$^+$ T cells, whereas *Il4*, *Il2*, and *Gata3* transcripts were equally present in WT and *Il27ra$^{-/-}$* cells (Figure 2A). Intracellular staining confirmed the enhanced IFN-γ production by *Il27ra*-deficient cells stimulated under non-polarizing conditions (Figure 2B). IFN-γ production by *Il27ra$^{-/-}$* and WT cells, however, was comparable under Th1 polarizing conditions (Figure 1-figure supplement 2H). The similar phenotype shared by *Il27p28* and *Il27ra* knockout mice indicates that the altered T cell functionality in the absence of IL-27p28 is indeed a reflection of disrupted IL-27Rα signaling.

3. IL-27p28 deficiency induces permissive epigenetic changes at *Ifng* and *Tbx21* loci

Developmentally regulated transcriptional activation and repression of genes or cell-type specific expression patterns are largely achieved by modifying the chromatin template at a gene locus (Ivashkiv, 2018). Murine neonatal $CD4^+$ T cells have been documented to be poised to rapid Th2 cytokine secretion due to the pre-existing hypomethylation at a key Th2 cytokine regulatory region (Rose, Lichtenheld, Foote, & Adkins, 2007). In other reports, Th2 polarization in adult SP thymocytes and RTEs is attributable to active recruitment of DNA methyltransferases and increased H3K4 methylation at *Il4* locus (Berkley et al., 2013; Makar et al., 2003). In addition, DNA methylation and histone modification are found to be important for the control of *Ifng* and *Tbx21* expression *(Fang et al., 2022; Friedman, Lee, Lee, & Oh, 2023; Jones & Chen, 2006)*. Therefore, we next evaluated the contribution of epigenetic modifications to the enhanced IFN-γ production in the absence of IL-27p28. Firstly, we performed bisulfite genomic sequencing on DNA of CD4 SP thymocytes from *Cd11c-cre p28$^{f/f}$* mice and WT littermates. We focused on the nine CpG sites (Figure 3A) most proximal to the *Ifng* transcription start site, among which the -53 CpG has previously been suggested to play a key role in IFN-γ repression in Th2 effector cells (Jones & Chen, 2006). DNA methylation was significantly reduced at three CpG sites (-53, -34 and +16 site) of the *Ifng* locus in CD4SP thymocytes from*Cd11c-cre p28$^{f/f}$* mice (Figure 3B). On the contrary, the five CpG sites in the *Il4* promoter region (Figure 3C, D), whose

demethylation is associated with high level IL-4 production (Lee, Agarwal, & Rao, 2002), showed no difference between cKO and WT CD4SP thymocytes.

As much as histone modifications are concerned, histone H3 lysine 27 trimethylation (H3K27me3) and H3 lysine 9 trimethylation (H3K9me3) are typically associated with repressed *Ifng* and *Tbx21* expression in Th cells, whereas histone H3 lysine 4 trimethylation (H3K4me3) enhances gene expression (Fang et al., 2022; Friedman et al., 2023). To evaluate the histone trimethylation modifications at *Ifng*, *Tbx21*, *Il4* and *Gata3* loci in CD4SP thymocytes from WT and *Cd11c-p28*$^{f/f}$ mice, chromatin immunoprecipitation was performed using antibodies against H3K4me3, H3K9me3 and H3K27me3. H3K4me3 was found to be accumulated at *Ifng* and *Tbx21* loci in cKO CD4SP thymocytes, while its level in *Gata3* and *Il4* loci was comparable to that of wild type cells (Figure 3E). On the other hand, neither the occupancy of H3K9me3 and H3K27me3 at *Ifng*, *Tbx21*, *Il4* and *Gata3* loci was altered (Figure 3F, G), nor were the total protein levels of H3K4me3, H3K9me3 H3K27me3 or the mRNA level of enzymes catalyzing the formation of these modifications (Figure 3-figure supplement 1A-C). These results suggest a link between up-regulated *Ifng* and *Tbx21* expression and altered epigenetic modifications in the absence of IL-27p28.

4. Coordinated up-regulation of STAT1-activated genes in CD4SP thymocytes from *Cd11c-p28*$^{f/f}$mice

To better understand the molecular mechanisms underlying the altered functionality, the transcriptional profile of CD4SP thymocytes from *Cd11c-p28*$^{f/f}$ mice

221 was explored by RNA-Seq and compared with that of the WT counterparts. The two
222 sets of differentially expressed genes (DEGs) were subjected to analyses for gene
223 ontology (GO) biological process terms and Kyoto Encyclopedia of Genes and
224 Genomes (KEGG) pathways. The up-regulated DEGs showed significant enrichment
225 in genes related to host defense to viral infection, including interferon response and Jak-
226 STAT signaling (Figure 4A). No meaningful hit, on the other hand, was revealed for the
227 down-regulated gene set (data not shown).

228 Given that STAT1 is a key mediator downstream of IL-27 signaling (Philips et al.,
229 2022), we were particularly interested in the altered expression of STAT1-regulated
230 genes in the absence of IL-27p28. A previous study by Hirahara et al. (Hirahara et al.,
231 2015) has compared the transcriptomes of wild-type and STAT1-deficient $CD4^+$ T cells
232 stimulated by IL-27. Using their data (GSE65621), we compiled a list of genes
233 potentially under regulation of STAT1. The DEGs were then examined for overlaps
234 with this gene set. Surprisingly, over 50% of up-regulated DEGs (69 out of 137) fell
235 into the category of STAT1-activated genes, whereas none of them belonged to STAT1-
236 suppressed genes (Figure 4B). To validate the RNA-Seq data, qPCR was carried out for
237 a group of overlapping genes, including *Gm12250, Oasl2, Oas3, Parp14, Ifit3, Usp18,*
238 *Igtp, Irf1, Ifi44, Oas2, Rsad2, Il12r*. As shown in Figure 4C, all these genes showed
239 differential expression between WT and cKO CD4SP thymocytes. To further illustrate
240 modest but coordinate changes in the expression of STAT1-regulated genes, gene set
241 enrichment analysis (GSEA) was performed without imposing an arbitrary fold-change
242 cutoff. Indeed, significant enrichment of STAT1-activated genes was detected in the

243 transcriptome of CD4SP thymocytes from the knockout mice (NES=1.67, NOM p-
244 val=10^{-16}, Figure 4D). Therefore, IL-27p28 deficiency resulted in an enhanced STAT1
245 activity.

246 To reveal functionally important connections of the DEGs, protein-protein
247 interaction network was generated using Network Analyst (Xia, Gill, & Hancock, 2015).
248 After removal of isolated and loosely connected nodes, the rest of the proteins encoded
249 by the DEGs were imported into Network Analyst for network construction. As shown
250 in Figure 4E, STAT1 was centrally positioned in the network with the highest degree of
251 interactions. Taken together, these results indicate that IL-27p28 deficiency is strongly
252 associated with an altered transcriptional program featured by enhanced expression of
253 STAT1-activated genes.

254

255 **5. Constitutive activation of STAT1 in CD4SP thymocytes in the absence of IL-**
256 **27p28**

257 The distinct transcriptional signature prompted us to examine the activation status
258 of STAT1 in freshly isolated CD4SP thymocytes from *Cd11c-p28*$^{f/f}$ mice and the WT
259 littermates. Total thymocytes were stained for CD4 and CD8, followed by intracellular
260 staining with antibodies against phosphorylated STATs. Significant levels of STAT1
261 Y701 phosphorylation were observed in cKO but not in WT cells. On the other hand,
262 both cKO and WT cells were stained negative for phosphorylated STAT3 and STAT4
263 (Figure 5A). Phosphorylated and total STAT proteins were also analyzed by Western
264 blotting in purified CD4SP thymocytes, RTEs and naive $CD4^+$ T cells. While the total

265 protein of STAT1 was comparable between cKO and WT cells in all populations
266 examined, elevated levels of phosphorylated STAT1 Y701 were constantly detected in
267 cKO cells. Moreover, the phosphorylation of STAT1 Y701 appeared to be
268 developmentally regulated, increasing progressively from CD4SP thymocytes to naive
269 T cells (Figure 5B). Another predominant phosphorylation site in STAT1 is serine 727,
270 which is crucial for maximal STAT1 transcription activity (Barnholt, Kota, Aung, &
271 Rutledge, 2009). Basal levels of S727 phosphorylation were also observed in CD4SP
272 thymocytes, but with no difference in WT and cKO cells (data not shown). As much as
273 STAT3 and STAT4 were concerned, neither total nor phosphorylated STAT3 and STAT4
274 were found to be altered with IL-27p28 ablation (Figure 5B), indicating that the impact
275 is specific for STAT1.

276 STAT1 plays an important role in the development of Th1 response by regulating
277 *Tbx21* and *Ifng* expression (Fang et al., 2022). To explore the correlation of the
278 increased STAT1 activation with the enhanced T-bet expression and IFN-γ production,
279 we assessed STAT1 binding on the *Tbx21* and *Ifng* loci by ChIP assay. Possibly due to
280 the relatively low abundance of activated STAT1, poor consistency was observed from
281 one experiment to another with freshly isolated CD4SP thymocytes. Therefore, we
282 chose to treat the cells with anti-CD3 and anti-CD28 for 3 days prior to the assay. Under
283 such conditions, STAT1 was found to be markedly accumulated in the promoter and
284 regulatory regions of both *Tbx21* and *Ifng* loci of cKO mice (Figure 5C). Notably, there
285 were strong positive correlations between the levels of STAT1 binding and H3K4me3
286 (Pearson's correlation coefficient for *Ifng* locus $r = 0.917$, $p = 0.010$ and *Tbx21* locus r

= 0.991, p <0.001, Figure 5D), indicating the implication of STAT1 in the epigenetic modifications of the loci. Together, these data suggest that IL-27p28-medaited signal normally imposes an inhibitory effect on STAT1 activation, which in turn helps the establishment of functional bias against the Th1 lineage.

6. Augmented autoimmune phenotype of *Aire*-deficient mice in the absence of IL-27p28

The physiological significance remains elusive of the bias against the Th1 effector functions for CD4SP thymocytes and RTEs. One hypothesis proposes that it favors the development of peripheral tolerance by avoiding a more inflammatory and potential detrimental response to self-antigens (Cunningham, Helm, & Fink, 2018; Fink & Hendricks, 2011; Hendricks & Fink, 2011). The disruption of such a bias in *Cd11c-p28*$^{f/f}$ mice provided a good model to test this hypothesis. Flow cytometric analysis of the peripheral T cell compartment demonstrated a significant increase of CD44^{hi}CD62L^{-} activated T cells with a concomitant decrease of CD44^{lo}CD62L^{+} naive T cells in the cKO mice compared to the WT littermates (Figure 6A). Nevertheless, the cKO mice displayed no obvious signs of autoimmunity up to the age of 24-30 weeks when assessed by auto-antibodies against double-strand DNA (Figure 6B) and tissue pathology (Figure 6C). Occasionally, small lymphoid foci were observed in the lung of cKO mice. But the CD4^{+} T cells recovered from the lung tissues displayed a similar cytokine secretion profile to that of WT mice except for the intrinsic augmentation of IFN-γ production (Figure 6D). Therefore, IL-27p28 deficiency alone is insufficient to

drive the development of autoimmunity.

We next sought to determine whether IL-27p28 deficiency would affect the autoimmune phenotype in the *Aire*$^{-/-}$ mouse, which are predisposed to developing autoimmunity due to a defect in clonal deletion of autoreactive T cells (van Laar, Hamburg, & Tas, 2022; J. X. Wang et al., 2021). To this end, *Cd11c-p28*$^{f/f}$ mice were crossed with *Aire*$^{-/-}$ mice to generate double knockout mice. Histological examination revealed increased lymphocyte infiltration and more severe structural distortion in the lung and stomach in double knockout mice in comparison to mice deficient for Aire only (Figure 6C). In addition, the double knockout mice exhibited an elevated level of autoantibodies to double-strand DNA, although the difference did not reach a statistical significance (p=0.068) possibly due to the limited sample size (Figure 6B). When CD4^{+} T cells recovered from the lung tissues were analyzed for IFN-γ, IL-4 and IL-17 production, the double knockout mice were virtually indistinguishable from the *Aire*$^{-/-}$ mice, except for increased IFN-γ production (Figure 6D).

Immunological anergy constitutes an important mechanism for peripheral tolerance. Two studies have identified a subset of naturally occurring Foxp3^{-}CD44^{hi}CD73^{hi}FR4^{hi} polyclonal CD4^{+} T cells in healthy hosts. They are enriched for self-antigen–specific T cell antigen receptors and represent functionally anergic cells (ElTanbouly & Noelle, 2021; Kalekar et al., 2016). We wondered whether the Th1 bias induced by IL-27p28 deficiency would affect the generation of the anergic population. As shown in Figure 6E, the CD4^{+}Foxp3^{-}CD44^{hi}CD73^{hi}FR4^{hi} anergic cells were significantly reduced in the double KO mice, which was accompanied by an

increase in the $CD4^{+}Foxp3^{-}CD44^{hi}CD73^{lo}FR4^{lo}$ effector/memory cells. Taken together, these data support that the bias against the Th1 lineage in newly generated T cells provides a unique mechanism to render autoreactive cells exquisitely sensitive to tolerance induction.

Discussion

Th2 polarization in adult SP thymocytes and RTEs is believed to be maintained through epigenetic modification at the *Il4* locus. However, the regulation of the opposing cytokine IFN-γ in this context remains unclear. We reported here that thymic DC-derived IL-27p28 played a key role in the establishment of the repressive status of the *Ifng* locus in newly generated $CD4^+$ T cells. As such, the loss of IL-27p28 in DCs endowed these cells with increased capacity of INF-γ production upon TCR engagement. Transcriptome profiling demonstrated coordinated up-regulation of STAT1-activated genes in the absence of IL-27p28. Indeed, enhanced phosphorylation of STAT1 was observed in CD4SP thymocytes from *Cd11c-p28*$^{f/f}$ mice, which was accompanied by the accumulation of STAT1 at the promoter and enhancer regions of *Ifng* and *Tbx21*. Epigenetic analyses indicated reduced DNA methylation at the *Ifng* locus and increased trimethylation of H3K4 at both *Ifng* and *Tbx21* loci in the absence of IL-27p28. Moreover, the H3K4me3 modification was shown to be strongly correlated with STAT1 binding to these loci. These data support a hypothesis that the exposure of developing thymocytes to IL-27p28 induces repressive epigenetic changes at the *Ifng* and *Tbx21* loci, possibly through antagonizing STAT1 activation, ultimately leading to an attenuated IFN-γ response of newly generated CD4SP thymocytes.

The present study revealed a significantly elevated level of phosphorylated STAT1 and up-regulation of a variety of STAT1-regulated genes in CD4SP thymocytes from *Cd11c-p28*$^{f/f}$ mice, indicating that IL-27p28 plays an important role in the fine tuning of STAT1 signaling in the developing thymocytes (Twohig et al., 2019). As IL-

27 is known to activate multiple STAT proteins, including STAT1, STAT3, STAT4, and STAT5 following engagement of the gp130/IL-27Rα receptor (Hirahara et al., 2015; Philips et al., 2022), the hyperactivation of STAT1 in the absence of IL-27p28 is somehow unexpected. We examined the potential impact of IL-27 deficiency on the expression of suppressors of cytokine signaling 3 (SOCS3), which has been shown to have a regulatory role in IL-27 signaling (Owaki, Asakawa, Fukai, Mizuguchi, & Yoshimoto, 2006). Comparable levels of SOCS3 were detected in CD4SP thymocytes and naive $CD4^+$ T cells from *Cd11c-p28*$^{f/f}$ mice and their littermates (Figure 5-figure supplement 1). We also explored the possibility that the constitutive activation of STAT1 might be the secondary effect of enhanced IFN-γ production (Iwata et al., 2017; Singhania et al., 2019). Addition of IFN-γ antibodies to the culture of CD4SP thymocytes and naive $CD4^+$ T cells, however, showed no significant effect on phosphorylated STAT1 levels in knockout cells (Figure 5-figure supplement 2A-B). Thus, STAT1 hyperactivation is unlikely due to loss of SOCS3 expression or positive feedback of IFN-γ signaling. Of note, it has been previously demonstrated that IL-27p28 on its own can act as a natural antagonist of gp130-mediated signaling triggered by IL-6, IL-11 and IL-27 (Stumhofer et al., 2010). Consistent with this finding, Chong et al. reported that IL-27p28 was able to inhibit IL-27-induced Th1 differentiation by reducing the phosphorylation of STAT1 and STAT3 (Chong et al., 2014). Therefore, we speculate that IL-27p28 in the thymus may primarily functions to suppress STAT1 activation induced by other cytokines.

A recent study demonstrated that both recombinant murine and human IL-27

379 induced the expression of antiviral proteins *Oas1*, *Oas2*, *Oas3*, *Oasl1*, and *Oasl2* in
380 epidermal keratinocytes. IL-27 signaling leads to OAS2 expression in a manner
381 dependent on IL27Rα and STAT1, but independent of STAT2. Apart from their antiviral
382 activity, OAS proteins are also involved in cell growth, differentiation, and apoptosis
383 (Castelli et al., 1997; Huang et al., 2022; Salzberg et al., 1997). The genomic mutation
384 and methylation of most OAS genes have been shown to alter their expression levels,
385 which is associated with the levels of infiltrated $CD4^+$ T cells and $CD8^+$ T cells in the
386 tumor microenvironment (Gao et al., 2022). Secreted OAS2 has also been observed to
387 inhibit CD3 zeta chain expression in T cells (Dar et al., 2016). In our current study, we
388 observed an increase in the transcription of *Oasl2, Oas2*, and *Oas3* in CD4SP
389 thymocytes from *Cd11c-p28*$^{f/f}$ mice, indicating that IL-27p28 signaling also involved
390 in the fine-tuning of these OAS protein expressions. Whether these molecules play a
391 role in thymocyte development remains to be clarified.

392 The biased functionality of newly generated $CD4^+$ T cells has been proposed to be
393 important for the induction of peripheral tolerance to self-antigens (Cunningham et al.,
394 2018; Fink & Hendricks, 2011; Hendricks & Fink, 2011). Despite the much enhanced
395 capacity of IFN-γ production by $CD4^+$ T cells and a significant increase of
396 $CD44^{hi}CD62L^-$ activated T cells, *Cd11c-p28*$^{f/f}$ mice displayed no apparent signs of
397 autoimmunity under steady-state conditions. This is consistent with the result of our
398 previous study in which negative selection was found to proceed normally in *Cd11c-*
399 *p28*$^{f/f}$ mice using the RIP-mOVA and OT-II models (Tang et al., 2016). We further
400 interrogated the impact of the disrupted functional bias in *Aire*$^{-/-}$ mice. Aire induces

401 ectopic expression of self-antigens in medullary thymic epithelial cells to mediate
402 negative selection of autoreactive thymocytes. Its mutation causes a rare life-
403 threatening autoimmune disease affecting multiple organs (van Laar et al., 2022; J. X.
404 Wang et al., 2021). In comparison to *Aire*$^{-/-}$ mice, *Cd11c-p28*$^{f/f}$ *Aire*$^{-/-}$ mice showed
405 elevated levels of double-strand DNA autoantibodies, increased lymphocytes
406 infiltration, and reduced anergic cells. Therefore, although disruption of the functional
407 bias in newly generated T cells is not sufficient to drive autoimmunity, it accelerates
408 disease development in hosts poised for autoimmunity.

409 In further support of a direct link between IL-27 and Aire, a recent study revealed
410 that IL-27 production was inhibited in Aire-overexpressing murine dendritic cells (Zou
411 et al., 2021). The two subunits IL-27p28 and EBI3 of human IL-27 are usually
412 coordinately expressed in antigen-presenting cells, while mouse IL-27p28 can be
413 secreted independently to inhibit the activities of IL-27 signaling (Pflanz et al., 2002;
414 Stumhofer et al., 2010). The distinct production profile of IL-27p28 between humans
415 and mice and our finding of the critical role of IL-27p28 in the maintenance of
416 functional bias in newly generated CD4^{+} T cells may explain the much weaker
417 autoimmune phenotype in *Aire*$^{-/-}$ mice than *AIRE*-mutated human subjects. In addition,
418 recent studies have reported elevation of serum IL-27p28 (also known as IL-30) in
419 patients with prostate cancer (Sorrentino et al., 2019), psoriasis (Omar, Xinxin, Jiayi,
420 Hussain, & Biao, 2021), and obesity (Q. Wang et al., 2021). It would be interesting to
421 explore the involvement of altered functionality of newly generated CD4^{+} T cells under
422 these pathological conditions.

423 Taken together, our data demonstrate that DC-derived IL-27p28 serves as an
424 endogenous inhibitor for STAT1 hyper-activation in developing thymocytes. By
425 regulating DNA and H3K4 methylation levels at the promoter and transcription
426 regulatory regions of *Ifng* and *Tbx21*, it is critically involved in the establishment of the
427 functional bias against IFN-γ production by newly generated $CD4^+$ T cells. Disruption
428 of this mechanism exacerbates autoimmune phenotypes in hosts predisposed for
429 autoimmunity.
430

Materials and methods

Mice

C57BL/6 mice were obtained from the Vital River Laboratories (Beijing, China). *Cd11c-p28*$^{f/f}$ mice and *Il27ra*$^{-/-}$ mice on C57BL/6 background were kindly provided by Dr. Zhinan Yin from Jinan University (Guangzhou, China). FVB-Tg (Rag2-EGFP) 1Mnz/J mice were purchased from Jackson Laboratory (Bar Harbor, ME) and were backcrossed for 10 generations onto the C57BL/6 background (termed as RAG2p-EGFP in this paper). RAG2p-EGFP mice were bred with *Cd11c-p28*$^{f/f}$ mice to generate *Cd11c-p28*$^{f/f}$ RAG2p-EGFP mice. *Aire*$^{-/-}$ mice were generously provided by Yangxin Fu (University of Chicago, IL) and were bred with *Cd11c-p28*$^{f/f}$ mice to generate *Aire*$^{-/-}$ *Cd11c-p28*$^{f/f}$ mice. Mice were used at 6-8 weeks of age unless stated otherwise. All the animal procedures were conformed to the Chinese Council on Animal Care Guidelines and the study was approved by the ethics committee of Peking University Health Science Center with an approval number of LA2014178.

Antibodies and reagents

PE-Cy7-conjugated anti-mouse CD4 (RM4-5), PE- and APC-conjugated anti-mouse CD8a (53–6.7), APC-conjugated anti-mouse IL-2 (JES6-5H4), PE-Cy7-conjugated anti-mouse TNF-α (MP6-XT22), PE-conjugated anti-mouse Stat1 (pY701) (4a), PerCP-Cy5.5-conjugated anti-mouse Stat3 (pY705) (4/P-STAT3), Alexa Fluor 488-conjugated anti-mouse Stat4 (pY693) (38/p-Stat4) were purchased from BD Biosciences (San Diego, CA). PE- and APC-conjugated anti-mouse CD25 (PC61.5)

453 and CD44 (IM7), FITC-conjugated anti-mouse FR4 (eBio12A5), PerCP-eFluor710-
454 conjugated anti-mouse CD73 (eBioTY/11.8), FITC-conjugated anti-mouse IL-4
455 (BVD6-24G2), PE-conjugated anti-mouse IL-17A (eBio17B7), APC-conjugated anti-
456 mouse FOXP3 (3G3), biotin-conjugated anti-mouse CD8a (53–6.7) and anti-phospho-
457 STAT-1(S727) were obtained from eBioscience (Waltham, MA). PE-conjugated anti-
458 mouse IFN-γ (XMG1.2) and PerCP-Cy5.5-conjugated anti-mouse T-bet (4B10) were
459 purchased from BioLegend (San Diego, CA).

460 Functional grade monoclonal antibodies for murine CD3 (145-2C11) and CD28
461 (37.51) and neutralizing anti-IL4 (11B11), neutralizing anti-IFN-γ (clone XMG1.2)
462 were obtained from eBioscience (Waltham, MA). Recombinant murine IL-2, IL-4, IL-
463 6, IL-12 and recombinant human TGF-β1 were purchased from R&D Systems
464 (Abingdon, UK).

465 Anti-phospho-STAT1(Tyr701), anti-STAT1, anti-phospho-STAT3 (Tyr705), anti-
466 STAT3, anti-phospho-STAT4 (Tyr693), anti-STAT4, anti-SOCS3, anti-Actin and HRP-
467 labeled goat-anti-rabbit or anti-mouse IgGs for Western blot assay were purchased from
468 Cell Signaling Technology (Danvers, MA). Phorbol 12-myristate 13-acetate (PMA) and
469 ionomycin were obtained from Sigma-Aldrich.

470

471 **Cell sorting and $CD4^+$ T-cell differentiation *in vitro***

472 To enrich CD4SP thymocytes, $CD8^-$ thymocytes were obtained by negative
473 selection using anti-CD8 (Ly-2) MicroBeads (Miltenyi Biotec). The cells were then
474 stained with fluorescently labeled antibodies to CD4, CD8 and CD44. $CD4^+$SP

475 thymocytes with the phenotype of $GFP^{+}CD4^{+}CD8^{-}CD44^{lo}$ were then sorted. For the
476 isolation of $CD4^{+}$ RTEs and mature naive $CD4^{+}$ T cells, $GFP^{+}CD4^{+}CD8^{-}CD25^{-}NK1.1^{-}$
477 (RTEs) and $GFP^{-}CD4^{+}CD8^{-}CD25^{-}CD44^{lo}$ (naive T) cells were sorted from lymph
478 nodes. All these cells were sorted to > 99% purity with a FACS Aria II (BD Biosciences,
479 San Diego, CA).

480 For *in vitro* activation, CD4SP thymocytes, RTEs and mature naive T cells were
481 cultured at a density of 2×10^{6}/mL with plate-coated anti-CD3 (clone 2C11; 2 μg/mL)
482 and soluble anti-CD28 (clone 37N; 1 μg/mL) in RPMl 1640 medium supplemented
483 with 10% fetal bovine serum (Biochrom Ag, Berlin), penicillin, streptomycin and 50
484 μM 2-mercaptoethanol. Conditions for $CD4^{+}$ T-cell differentiation were as follows: Th0
485 cells, IL-2 (2 ng/mL); Th1 cells, IL-12 (10 ng/mL), IL-2 (2 ng/mL), anti-IL-4 (10
486 μg/mL); Th2 cells, IL-4 (20 ng/mL), IL-2 (2 ng/mL), anti-IFN-γ (10 μg/mL); Th17
487 cells, recombinant human TGFβ1 (10 ng/mL), IL-6 (10 ng/mL), anti-IL-4 (10 μg/mL),
488 anti-IFN-γ (10 μg/mL); and Treg cells, TGFβ1 (1 ng/mL), IL-2 (10 ng/mL), anti-IL-4
489 (10 μg/mL), anti-IFN-γ (10 μg/mL). After 3 days of differentiation, supernatants were
490 collected and cells were subjected to intracellular cytokine staining and flow cytometry
491 analyses.

492

493 **Intracellular staining and flow cytometry**

494 For detection of surface molecules, T cells were labelled with the appropriate
495 fluorescent mAbs on ice for 30 min. For detection of cytoplasmic molecules, T-bet, and
496 FOXP3, T cells were collected, stained with surface molecules, fixed, permeabilized

497 with the Foxp3/Transcription Factor Staining Buffer (eBioscience), and stained with
498 fluorochrome-conjugated mouse antibodies on ice for 30 min. For intracellular cytokine
499 staining, five hours before harvest, T cells were stimulated with PMA (50 ng/mL) plus
500 ionomycin (1 mg/mL) in the presence of a protein transport inhibitor, monensin (2 μM)
501 or BFA (3 μg/mL) (eBioscience). Cells were collected, washed, fixed, permeabilized
502 (FIX AND PERM, Invitrogen) and stained with IFN-γ, IL-4, IL-2, TNF-α, and IL-17
503 antibodies according to the manufacturer's instructions. For detection of
504 phosphorylated STATs, 1×10^7 thymocytes were fixed for 10 min at 37°C with 2%
505 (wt/vol) paraformaldehyde. After fixing, cells were permeabilized for 30 min on ice
506 with 90% (vol/vol) methanol, and stained with the appropriate antibodies. Flow
507 cytometry was conducted on a Galios (Beckman Coulter) and data analysis was
508 performed using Kaluza software.
509

510 **Enzyme-Linked Immunosorbent Assay (ELISA)**

511 Supernatants of *in vitro* cell cultures were obtained at 72 hr. IFN-γ and IL-4
512 production were determined using ELISA kits (BioLegend, San Diego, CA) according
513 to the manufacturer's instructions.

514 For the analysis of anti-dsDNA antibodies, serum was collected from 24-30-week-
515 old *Aire*$^{-/-}$*Cd11c-Cre p28*$^{f/f}$, *Aire*$^{-/-}$, *Cd11c-Cre p28*$^{f/f}$ and WT mice. Nunc MaxiSorp
516 ELISA plates were precoated with dsDNA (100 mg/mL, Sigma, St. Louis, MO) in
517 phosphate-buffered saline (PBS) at 4˚C overnight. Plates were blocked with 5% BSA
518 for 1 hour at 37˚C, then washed and incubated with 1/100 dilutions of mouse sera for 2

519 hours at 37˚C. Plates were washed, and anti-dsDNA antibodies were detected with a
520 1/1000 dilution of alkaline phosphatase–conjugated goat anti-mouse IgG (BioLegend)
521 for 1 hour at 37˚C and developed with a phosphatase substrate for 30 min at 37˚C.
522

523 **Quantitative PCR (qPCR)**

524 RNA was purified from various T cell subsets cultured under Th0 conditions for
525 12 h using Trizol reagent (Invitrogen). cDNA was synthesized using reverse
526 transcription kit (Progema). qPCR was performed using FastStart Universal SYBR
527 Green Master mix (Roche, Basel, Switzerland) on an iCycler real-time PCR system
528 (Bio-Rad Laboratories, Hemel Hempstead, U.K.), with each sample in triplicate. The
529 quantification was based on delta delta CT calculations and was normalized to β-actin
530 as loading controls. The primers used in the study were listed in Supplementary Table
531 1.
532

533 **DNA methylation**

534 Bisulfite modification of genomic DNA from FACS purified cells was performed
535 using the EZ DNA methylation kit (Zymo Research). For methylation analysis on *Ifng*
536 gene promoter CpG sites, bisulfite-treated DNA was amplified in semi-nested PCR
537 using primers: 5'-GGTGTGAAGTAAAAGTGTTTTTAGAGAATTTTAT-3' and 5'-
538 CAATAACAACCAAAAACAACCATAAAAAAAAACT-3', then 5'-
539 GGTGTGAAGTAAAAGTGTTTTTAGAGAATTTTAT-3' and 5'-
540 CCATAAAAAAAAACTACAAAACCAAAATACAATA-3'. For methylation analysis

541 on *Il4* gene promoter CpG sites, bisulfite-treated DNA was amplified in PCR using
542 primers: 5-GGATCCACACGGTGCAAAGAGAGACCC-3' and 5′-
543 TCGGCCTTTCAGACTAATCTTATCAGC-3' The PCR products were gel purified
544 and cloned into the pGEM-T vector (Promega; Madison, WI, USA). The inserted PCR
545 fragments of individual clones were sequenced by Tsing KE Biological Technology,
546 Beijing, China. For all samples, 10 reads per CpG site were used to determine the
547 average percentage of methylated CpG.
548

549 **Chromatin immunoprecipitation (ChIP)**

550 ChIP assays were carried out by using Pierce Agarose Chip Kit (Pierce
551 Biotechnology). Briefly, cells were cross-linked for 10 min with 1% formaldehyde and
552 lysed with Nuclease. 10% of the digested chromatin was preserved as input control and
553 the rest of the digested chromatin were incubated with specific antibody or normal IgG
554 (as a control). The purified DNA from immunoprecipitation and the input samples were
555 analyzed by qPCR using primers specific listed in Supplementary Table 1. Data is
556 presented as a percent input of each IP sample relative to input chromatin. The
557 following antibodies were used in ChIP analysis: H3K4me3 (Millipore), H3K27me3
558 (Millipore), H3K9me3 (Abcam), and STAT1 (Cell Signaling Technology).
559

560 **Western blotting**

561 For short term TCR stimulation, CD4SP thymocytes and mature naive T cells were
562 incubated with 2 μg/mL anti-mouse CD3 and 1 μg/mL anti-mouse CD28 on ice for 20

563 min, followed by cross-linking for 10 min at 37°C with 5 μg/mL goat-anti-hamster IgG.
564 Cells were then washed with PBS. Freshly isolated T cells or stimulated T cells were
565 lysed in RIPA buffer for 30 minutes. Whole-cell lysates (5–10 μg per sample) were
566 separated by SDS/PAGE and analyzed by immunoblotting with antibodies to phospho-
567 STAT-1 (Tyr701), phospho-STAT-1 (Ser727), STAT-1, phospho-STAT-3 (Tyr705),
568 STAT-3, phospho-STAT-4 (Tyr693), STAT-4, SOCS3 and Actin. HRP-conjugated anti-
569 Rabbit IgG was used as the detection antibody. The bands were quantified using ImageJ
570 software.
571
572 **RNA-seq**
573 Total RNA was extracted from approximately 2×10^6 CD4SP thymocytes from WT
574 and *Cd11c-p28*$^{f/f}$ mice using Trizol reagent (Invitrogen). Each sample was a mixture of
575 equal amounts of CD4SP thymocytes from three mice. RNA underwent quality control
576 testing using a bionalayser followed by cDNA library preparation. Library construction
577 and sequencing on Illumina HiSEq 2000 were performed by BIOPIC, Peking
578 University.
579
580 **H&E**
581 Organs from 24-30-week-old *Aire*$^{-/-}$*Cd11c-p28*$^{f/f}$ mice, *Aire*$^{-/-}$ mice and WT mice
582 were collected and fixed overnight in 10% formalin, embedded in paraffin, sectioned
583 and stained with hematoxylin and eosin (H&E). The degree of lymphocytic infiltrates

was analyzed in a blinded fashion. In general, 0, 1, 2 and 3 indicate no, mild, moderate, or severe lymphocytic infiltration, respectively.

Statistical analysis

Data are reported as the mean ± Standard deviation (SD). Differences between groups were analyzed by Student's *t* test or two-way Anova (for multiple variant comparisons) using GraphPad Prism software (GraphPad). Throughout the text, figures, and figure legends, the following terminology is used to denote statistical significance: * $P<0.05$, ** $P<0.01$. *** $P<0.001$. NS, not significant.

Ashby, K. M., & Hogquist, K. A. (2023). A guide to thymic selection of T cells. *Nat Rev Immunol*. doi:10.1038/s41577-023-00911-8

Barnholt, K. E., Kota, R. S., Aung, H. H., & Rutledge, J. C. (2009). Adenosine blocks IFN-gamma-induced phosphorylation of STAT1 on serine 727 to reduce macrophage activation. *Journal of Immunology, 183*(10), 6767-6777. doi:10.4049/jimmunol.0900331

Berkley, A. M., Hendricks, D. W., Simmons, K. B., & Fink, P. J. (2013). Recent Thymic Emigrants and Mature Naive T Cells Exhibit Differential DNA Methylation at Key Cytokine Loci. *Journal of Immunology, 190*(12), 6180-6186. doi:10.4049/jimmunol.1300181

Bhaumik, S., Giffon, T., Bolinger, D., Kirkman, R., Lewis, D. B., Weaver, C. T., & Randolph, D. A. (2013). Retinoic Acid Hypersensitivity Promotes Peripheral Tolerance in Recent Thymic Emigrants. *Journal of Immunology, 190*(6), 2603-2613. doi:10.4049/jimmunol.1200852

Cao, Y. X., Doodes, P. D., Glant, T. T., & Finnegan, A. (2008). IL-27 induces a Th1 immune response and susceptibility to experimental arthritis. *Journal of Immunology, 180*(2), 922-930. doi:DOI 10.4049/jimmunol.180.2.922

Castelli, J. C., Hassel, B. A., Wood, K. A., Li, X. L., Amemiya, K., Dalakas, M. C., . . . Youle, R. J. (1997). A study of the interferon antiviral mechanism: apoptosis activation by the 2-5A system. *J Exp Med, 186*(6), 967-972. doi:10.1084/jem.186.6.967

Caveney, N. A., Glassman, C. R., Jude, K. M., Tsutsumi, N., & Garcia, K. C. (2022). Structure of the IL-27 quaternary receptor signaling complex. *Elife, 11*. doi:10.7554/eLife.78463

Chong, W. P., Horai, R., Mattapallil, M. J., Silver, P. B., Chen, J., Zhou, R., . . . Caspi, R. R. (2014). IL-27p28 inhibits central nervous system autoimmunity by concurrently antagonizing Th1 and Th17 responses. *J Autoimmun, 50*, 12-22. doi:10.1016/j.jaut.2013.08.003

Cunningham, C. A., Helm, E. Y., & Fink, P. J. (2018). Reinterpreting recent thymic emigrant function: defective or adaptive? *Curr Opin Immunol, 51*, 1-6. doi:10.1016/j.coi.2017.12.006

Dar, A. A., Pradhan, T. N., Kulkarni, D. P., Shah, S. U., Rao, K. V., Chaukar, D. A., . . . Chiplunkar, S. V. (2016). Extracellular 2'5'-oligoadenylate synthetase 2 mediates T-cell receptor CD3-zeta chain down-regulation via caspase-3 activation in oral cancer. *Immunology, 147*(2), 251-264. doi:10.1111/imm.12560

Diveu, C., McGeachy, M. J., Boniface, K., Stumhofer, J. S., Sathe, M., Joyce-Shaikh, B., . . . Kastelein, R. A. (2009). IL-27 Blocks RORc Expression to Inhibit Lineage Commitment of Th17 Cells. *Journal of Immunology, 182*(9), 5748-5756. doi:10.4049/jimmunol.0801162

ElTanbouly, M. A., & Noelle, R. J. (2021). Rethinking peripheral T cell tolerance: checkpoints across a T cell's journey. *Nature Reviews Immunology, 21*(4), 257-267. doi:10.1038/s41577-020-00454-2

Fang, D., Healy, A., & Zhu, J. (2022). Differential regulation of lineage-determining transcription factor expression in innate lymphoid cell and adaptive T helper cell subsets. *Front Immunol, 13*, 1081153. doi:10.3389/fimmu.2022.1081153

Fink, P. J., & Hendricks, D. W. (2011). Post-thymic maturation: young T cells assert their individuality. *Nature Reviews Immunology, 11*(8), 544-549. doi:10.1038/nri3028

Flores, R. R., Kim, E., Zhou, L., Yang, C., Zhao, J., Gambotto, A., & Robbins, P. D. (2015). IL-Y, a synthetic member of the IL-12 cytokine family, suppresses the development of type 1 diabetes in NOD mice. *European Journal of Immunology, 45*(11), 3114-3125. doi:10.1002/eji.201445403

Friedman, M. J., Lee, H., Lee, J. Y., & Oh, S. (2023). Transcriptional and Epigenetic Regulation of

Context-Dependent Plasticity in T-Helper Lineages. *Immune Netw, 23*(1), e5. doi:10.4110/in.2023.23.e5

Gao, L., Ren, R., Shen, J., Hou, J., Ning, J., Feng, Y., . . . Cao, J. (2022). Values of OAS gene family in the expression signature, immune cell infiltration and prognosis of human bladder cancer. *BMC Cancer, 22*(1), 1016. doi:10.1186/s12885-022-10102-8

Hamano, S., Himeno, K., Miyazaki, Y., Ishii, K., Yamanaka, A., Takeda, A., . . . Yoshida, H. (2003). WSX-1 is required for resistance to infection by regulation of proinflammatory cytokine production. *Immunity, 19*(5), 657-667. doi:Doi 10.1016/S1074-7613(03)00298-X

Harker, J. A., Wong, K. A., Dolgoter, A., & Zuniga, E. I. (2015). Cell-Intrinsic gp130 Signaling on CD4 T Cells Shapes Long-Lasting Antiviral Immunity. *Journal of Immunology, 195*(3), 1071-1081. doi:10.4049/jimmunol.1402402

Hendricks, D. W., & Fink, P. J. (2011). Recent thymic emigrants are biased against the T-helper type 1 and toward the T-helper type 2 effector lineage. *Blood, 117*(4), 1239-1249. doi:10.1182/blood-2010-07-299263

Hirahara, K., Onodera, A., Villarino, A. V., Bonelli, M., Sciumè, G., Laurence, A., . . . O'Shea, J. J. (2015). Asymmetric Action of STAT Transcription Factors Drives Transcriptional Outputs and Cytokine Specificity. *Immunity, 42*(5), 877-889. doi:10.1016/j.immuni.2015.04.014

Huang, Y. Z., Zheng, Y. X., Zhou, Y., Xu, F., Cui, Y. Z., Chen, X. Y., . . . Man, X. Y. (2022). OAS1, OAS2, and OAS3 Contribute to Epidermal Keratinocyte Proliferation by Regulating Cell Cycle and Augmenting IFN-1−Induced Jak1−Signal Transducer and Activator of Transcription 1 Phosphorylation in Psoriasis. *J Invest Dermatol, 142*(10), 2635-2645 e2639. doi:10.1016/j.jid.2022.02.018

Huber, M., Steinwald, V., Guralnik, A., Brüstle, A., Kleemann, P., Rosenplänter, C., . . . Lohoff, M. (2008). IL-27 inhibits the development of regulatory T cells via STAT3. *Wiener Klinische Wochenschrift, 120*, 45-45.

Ivashkiv, L. B. (2018). IFNgamma: signalling, epigenetics and roles in immunity, metabolism, disease and cancer immunotherapy. *Nat Rev Immunol, 18*(9), 545-558. doi:10.1038/s41577-018-0029-z

Iwata, S., Mikami, Y., Sun, H. W., Brooks, S. R., Jankovic, D., Hirahara, K., . . . Kanno, Y. (2017). The Transcription Factor T-bet Limits Amplification of Type I IFN Transcriptome and Circuitry in T Helper 1 Cells. *Immunity, 46*(6), 983-+. doi:10.1016/j.immuni.2017.05.005

Jones, B., & Chen, J. (2006). Inhibition of IFN-gamma transcription by site-specific methylation during T helper cell development. *EMBO J, 25*(11), 2443-2452. doi:10.1038/sj.emboj.7601148

Kalekar, L. A., Schmiel, S. E., Nandiwada, S. L., Lam, W. Y., Barsness, L. O., Zhang, N., . . . Mueller, D. L. (2016). CD4(+) T cell anergy prevents autoimmunity and generates regulatory T cell precursors. *Nat Immunol, 17*(3), 304-314. doi:10.1038/ni.3331

Kim, D., Le, H. T., Nguyen, Q. T., Kim, S., Lee, J., & Min, B. (2019). Cutting Edge: IL-27 Attenuates Autoimmune Neuroinflammation via Regulatory T Cell/Lag3-Dependent but IL-10-Independent Mechanisms In Vivo. *Journal of Immunology, 202*(6), 1680-1685. doi:10.4049/jimmunol.1800898

Lee, D. U., Agarwal, S., & Rao, A. (2002). Th2 lineage commitment and efficient IL-4 production involves extended demethylation of the IL-4 gene. *Immunity, 16*(5), 649-660. doi:10.1016/s1074-7613(02)00314-x

Lin, T. T., Lu, J., Qi, C. Y., Yuan, L., Li, X. L., Xia, L. P., & Shen, H. (2015). Elevated serum level of IL-27 and VEGF in patients with ankylosing spondylitis and associate with disease activity. *Clinical and Experimental Medicine, 15*(2), 227-231. doi:10.1007/s10238-014-0281-x

Liu, J. Q., Liu, Z. Z., Zhang, X. J., Shi, Y., Talebian, F., Carl, J. W., . . . Bai, X. F. (2012). Increased Th17 and Regulatory T Cell Responses in EBV-Induced Gene 3-Deficient Mice Lead to Marginally Enhanced Development of Autoimmune Encephalomyelitis. *Journal of Immunology, 188*(7), 3099-3106. doi:10.4049/jimmunol.1100106

Makar, K. W., Perez-Melgosa, M., Shnyreva, M., Weaver, W. M., Fitzpatrick, D. R., & Wilson, C. B. (2003). Active recruitment of DNA methyltransferases regulates interleukin 4 in thymocytes and T cells. *Nat Immunol, 4*(12), 1183-1190. doi:10.1038/ni1004

Mei, Y. W., Lv, Z., Xiong, L. L., Zhang, H. W., Yin, N. L., & Qi, H. B. (2021). The dual role of IL-27 in CD4+T cells. *Molecular Immunology, 138*, 172-180. doi:10.1016/j.molimm.2021.08.001

Neufert, C., Becker, C., Wirtz, S., Fantini, M. C., Weigmann, B., Galle, P. R., & Neurath, M. F. (2007). IL-27 controls the development of inducible regulatory T cells and Th17 cells via differential effects on STAT1. *European Journal of Immunology, 37*(7), 1809-1816. doi:10.1002/eji.200636896

Nguyen, Q. T., Jang, E., Le, H. T., Kim, S., Kim, D., Dvorina, N., . . . Min, B. (2019). IL-27 targets Foxp3 Tregs to mediate antiinflammatory functions during experimental allergic airway inflammation. *Jci Insight, 4*(2). doi:10.1172/jci.insight.123216

Omar, N. S., Xinxin, L., Jiayi, X., Hussain, S. G., & Biao, P. X. (2021). Serum level of cytokine IL-30 in psoriatic patients and correlation with disease severity. *J Popul Ther Clin Pharmacol, 28*(1), 24-33. doi:10.15586/jptcp.2021.v28i1.823

Owaki, T., Asakawa, M., Fukai, F., Mizuguchi, J., & Yoshimoto, T. (2006). IL-27 induces Th1 differentiation via p38 MAPK/T-bet- and intercellular adhesion molecule-1/LFA-1/ERK1/2-dependent pathways. *Journal of Immunology, 177*(11), 7579-7587. doi:10.4049/jimmunol.177.11.7579

Park, J., DeLong, J. H., Knox, J. J., Konradt, C., Wojno, E. D. T., & Hunter, C. A. (2019). Impact of Interleukin-27p28 on T and B Cell Responses during Toxoplasmosis. *Infection and Immunity, 87*(12). doi:10.1128/IAI.00455-19

Park, Y. J., Ryu, H., Choi, G., Kim, B. S., Hwang, E. S., Kim, H. S., & Chung, Y. (2019). IL-27 confers a protumorigenic activity of regulatory T cells via CD39. *Proceedings of the National Academy of Sciences of the United States of America, 116*(8), 3106-3111. doi:10.1073/pnas.1810254116

Pflanz, S., Timans, J. C., Cheung, J., Rosales, R., Kanzler, H., Gilbert, J., . . . Kastelein, R. A. (2002). IL-27, a heterodimeric cytokine composed of EBI3 and p28 protein, induces proliferation of naive CD4+ T cells. *Immunity, 16*(6), 779-790. doi:10.1016/s1074-7613(02)00324-2

Philips, R. L., Wang, Y., Cheon, H., Kanno, Y., Gadina, M., Sartorelli, V., . . . O'Shea, J. J. (2022). The JAK-STAT pathway at 30: Much learned, much more to do. *Cell, 185*(21), 3857-3876. doi:10.1016/j.cell.2022.09.023

Rose, S., Lichtenheld, M., Foote, M. R., & Adkins, B. (2007). Murine neonatal CD4+ cells are poised for rapid Th2 effector-like function. *Journal of Immunology, 178*(5), 2667-2678. doi:10.4049/jimmunol.178.5.2667

Salzberg, S., Hyman, T., Turm, H., Kinar, Y., Schwartz, Y., Nir, U., . . . Huberman, E. (1997). Ectopic expression of 2-5A synthetase in myeloid cells induces growth arrest and facilitates the

appearance of a myeloid differentiation marker. *Cancer Res, 57*(13), 2732-2740.

Shen, H., Xia, L. P., & Lu, J. (2013). Elevated levels of interleukin-27 and effect on production of interferon-γ and interleukin-17 in patients with Behcet's disease. *Scandinavian Journal of Rheumatology, 42*(1), 48-51. doi:10.3109/03009742.2012.704391

Singhania, A., Graham, C. M., Gabrysová, L., Moreira-Teixeira, L., Stavropoulos, E., Pitt, J. M., . . . O'Garra, A. (2019). Transcriptional profiling unveils type I and II interferon networks in blood and tissues across diseases. *Nature Communications, 10*. doi:ARTN 288710.1038/s41467-019-10601-6

Sorrentino, C., Yin, Z., Ciummo, S., Lanuti, P., Lu, L. F., Marchisio, M., . . . Di Carlo, E. (2019). Targeting Interleukin(IL)-30/IL-27p28 signaling in cancer stem-like cells and host environment synergistically inhibits prostate cancer growth and improves survival. *J Immunother Cancer, 7*(1), 201. doi:10.1186/s40425-019-0668-z

Stumhofer, J. S., Tait, E. D., Quinn, W. J., Hosken, N., Spudy, B., Goenka, R., . . . Hunter, C. A. (2010). A role for IL-27p28 as an antagonist of gp130-mediated signaling. *Nature Immunology, 11*(12), 1119-U1118. doi:10.1038/ni.1957

Tang, H., Zhang, J., Sun, X., Qian, X., Zhang, Y., & Jin, R. (2016). Thymic DCs derived IL-27 regulates the final maturation of CD4(+) SP thymocytes. *Sci Rep, 6*, 30448. doi:10.1038/srep30448

Tormo, A. J., Meliani, Y., Beaupré, L. A., Sharma, M., Fritz, J. H., Elson, G., . . . Gauchat, J. F. (2013). The Composite Cytokine p28/Cytokine-Like Factor 1 Sustains B Cell Proliferation and Promotes Plasma Cell Differentiation. *Journal of Immunology, 191*(4), 1657-1665. doi:10.4049/jimmunol.1201595

Twohig, J. P., Figueras, A. C., Andrews, R., Wiede, F., Cossins, B. C., Soria, A. D., . . . Jones, S. A. (2019). Activation of naive CD4 T cells re-tunes STAT1 signaling to deliver unique cytokine responses in memory CD4 T cells. *Nature Immunology, 20*(4), 458-+. doi:10.1038/s41590-019-0350-0

van Laar, G. G., Hamburg, J. P. V., & Tas, S. W. (2022). Extrathymic AIRE-expressing cells: Friends or foes in autoimmunity and cancer? *Autoimmunity Reviews, 21*(9). doi:10.1016/j.autrev.2022.103141

Villarino, A., Hibbert, L., Lieberman, L., Wilson, E., Mak, T., Yoshida, H., . . . Hunter, C. A. (2003). The IL-27R (WSX-1) is required to suppress T cell hyperactivity during infection. *Immunity, 19*(5), 645-655. doi:Doi 10.1016/S1074-7613(03)00300-5

Wang, J. X., Lareau, C. A., Bautista, J. L., Gupta, A. R., Sandor, K., Germino, J., . . . Gardner, J. M. (2021). Single-cell multiomics defines tolerogenic extrathymic Aire-expressing populations with unique homology to thymic epithelium. *Science Immunology, 6*(65). doi:10.1126/sciimmunol.abl5053

Wang, Q., Li, D., Cao, G., Shi, Q., Zhu, J., Zhang, M., . . . Yin, Z. (2021). IL-27 signalling promotes adipocyte thermogenesis and energy expenditure. *Nature, 600*(7888), 314-318. doi:10.1038/s41586-021-04127-5

Xia, J., Gill, E. E., & Hancock, R. E. (2015). NetworkAnalyst for statistical, visual and network-based meta-analysis of gene expression data. *Nat Protoc, 10*(6), 823-844. doi:10.1038/nprot.2015.052

Zhang, S., Liang, R. F., Luo, W., Liu, C., Wu, X. L., Gao, Y. A., . . . Yin, Z. N. (2013). High susceptibility to liver injury in IL-27 p28 conditional knockout mice involves intrinsic interferon-γ dysregulation of CD4 T cells. *Hepatology, 57*(4), 1620-1631. doi:10.1002/hep.26166

Zou, X. Y., Wang, S., Zhang, Y., Wang, X. Y., Zhang, R. C., Yang, W., & Li, Y. (2021). AIRE-overexpressing BMDCs suppress TFH cells through ICOSL to prevent and attenuate autoimmune diabetes in NOD mice. *International Immunopharmacology, 99*. doi:10.1016/j.intimp.2021.107979

Abbreviations

AS, ankylosing spondyliti; BD, behcet disease; ChIP, chromatin immunoprecipitation; cKO, conditional knockout; DC, dendritic cell; DEGs, differentially expressed genes; EAE, experimental autoimmune encephalomyelitis; EBI3, Epstein-Barr virus-induced gene 3; ELISA, Enzyme-Linked Immunosorbent Assay; GO, gene ontology; GSEA, gene set enrichment analysis; H3K4me3, histone H3 lysine 4 trimethylation; H3K27me3, histone H3 lysine 27 trimethylation; H3K9me3, histone H3 lysine 9 trimethylation; IFN-γ, interferon-γ; IL-2, interleukin 2; KEGG, Kyoto Encyclopedia of Genes and Genomes; PBS, phosphate-buffered saline; RTE, recent thymic emigrants; SOCS3, suppressors of cytokine signaling 3; SP, single-positive thymocyte; STAT, signal transducer and activator of transcription; T-bet, T-box transcription factor; Th, T helper; TNF-α, tumor necrosis factor α; WT, wild-type.

Author Contributions

JZ and RJ designed and carried out the study, collected and analyzed the data and drafted the manuscript. JZ and HT performed the phenotype analysis, epigenetic assay and established the mouse model. HMW analyzed the RNA-seq data. XWP performed the cell sorting assay. YZ conceived and designed the study, analyzed the data, and drafted the manuscript. All authors read and approved the final manuscript.

Acknowledgments

We thank Dr. Zhinan Yin from Jinan University (Guangzhou, China) for kindly

provided *Cd11c-cre p28*$^{flox/flox}$ mice and *Il27ra*$^{-/-}$ mice.

Conflicts of Interest

The authors declare no conflict of interest.

Funding

This work was supported by grants from the National Natural Sciences Foundation of China (32230037; 82394412; 32071178; 31872733), National Key Research and Development Program of China (2023YFB3507000) and Beijing Life Science Academy (2024600CC0080).

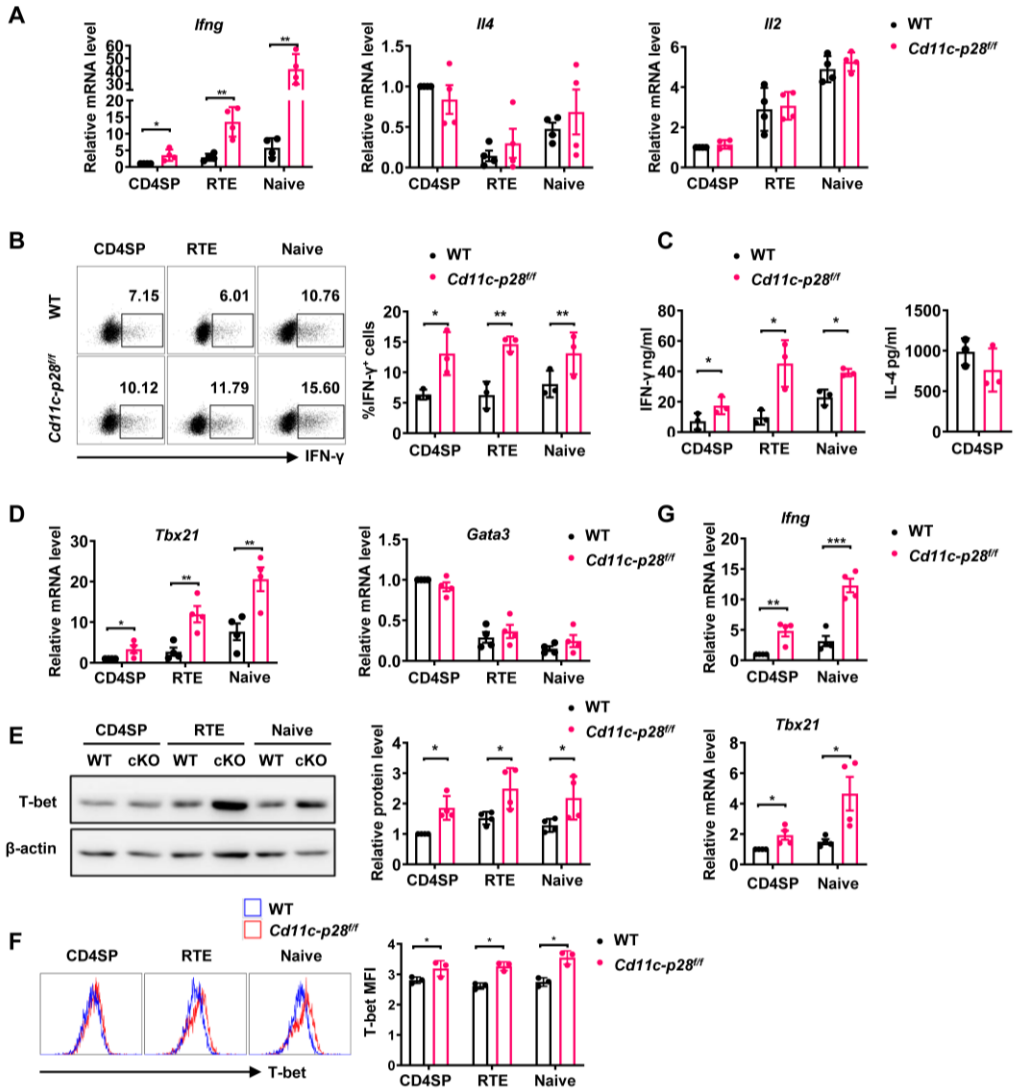

Figure 1. Elevated IFN-γ production and T-bet expression in *Cd11c-p28*$^{f/f}$ mice initiated from CD4SP thymocytes stage.

(A) CD4SP (GFP^{+}CD4^{+}CD8^{-}CD44^{lo}) thymocytes, CD4^{+} RTEs (GFP^{+}CD4^{+}CD8^{-}CD25^{-}CD44^{lo}) and CD4^{+} naive (GFP^{-}CD4^{+}CD8^{-}CD25^{-}CD44^{lo}) T cells were sorted from 6-8-week-old *Cd11c-p28*$^{f/f}$ mice and WT littermates, stimulated with plate coated anti-CD3 (2 μg/mL) and soluble anti-CD28 (1 μg/mL) for 12 hours. mRNA levels of *Ifng*, *Il4*, and *Il2* were determined by qPCR. Data: mean ± SD (n=4, duplicates).

(B) Sorted cells were cultured under Th0 conditions for 3 days. The frequency of IFN-γ-producing CD4^{+} T cells were measured by intracellular staining. Representative dot

plots (left) and statistical data (right, mean ± SD, n=3).

(C) Supernatants from 3-day cultures were analyzed for IFN-γ and IL-4 by ELISA. Data: mean ± SD (n=3).

(D) mRNA levels of *Tbx21* and *Gata3* in sorted cells were determined by qPCR. Data: mean ± SD (n=4, duplicates).

(E-F) T-bet protein levels were assessed by Western blot (E) and flow cytometry (F) after 3-day culture. Data: mean ± SD (n=3).

(G) Freshly sorted cells were lysed in Trizol, and *Ifng* and *Tbx21* mRNA levels were determined by qPCR. Data: mean ± SD (n=4, duplicates). Statistical differences: * $P < 0.05$, ** $P < 0.01$, *** $P < 0.001$ (Student's *t*-test).

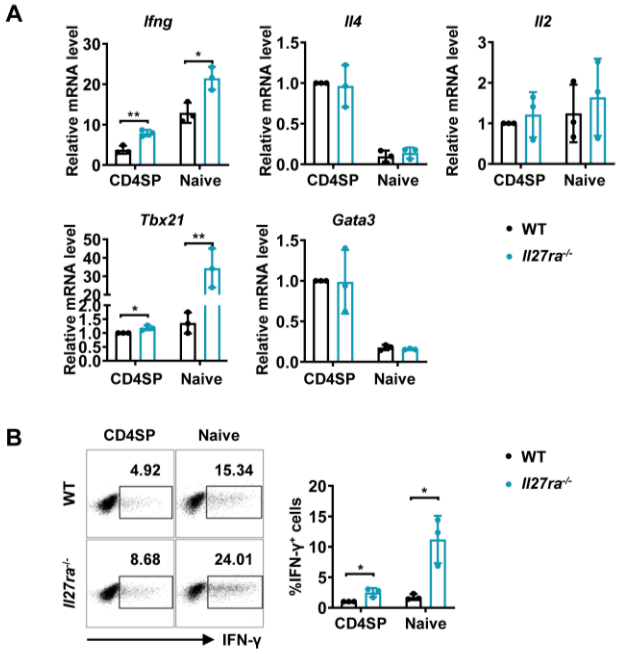

Figure 2. Enhanced IFN-γ production and T-bet expression in *Il27ra*$^{-/-}$ mice initiated at the CD4SP thymocytes stage.

(A) CD4SP thymocytes and naive CD4^{+} T cells were isolated from *Il27ra*$^{-/-}$ and WT mice, stimulated with plate-coated anti-CD3 (2 μg/mL) and soluble anti-CD28 (1 μg/mL) for 12 hours. mRNA levels of *Ifng*, *Il4*, *Il2*, *Tbx21*, and *Gata3* were determined by qPCR. Data: mean ± SD (n=3, duplicates).

(B) CD4SP thymocytes and CD4^{+} naive T cells were cultured under Th0 conditions for 3 days. The frequency of IFN-γ-producing CD4^{+} T cells were analyzed by intracellular staining. Representative dot plots (left) and quantification (right, mean ± SD, n=3). Significance: * $P < 0.05$, ** $P < 0.01$ (Student's *t*-test).

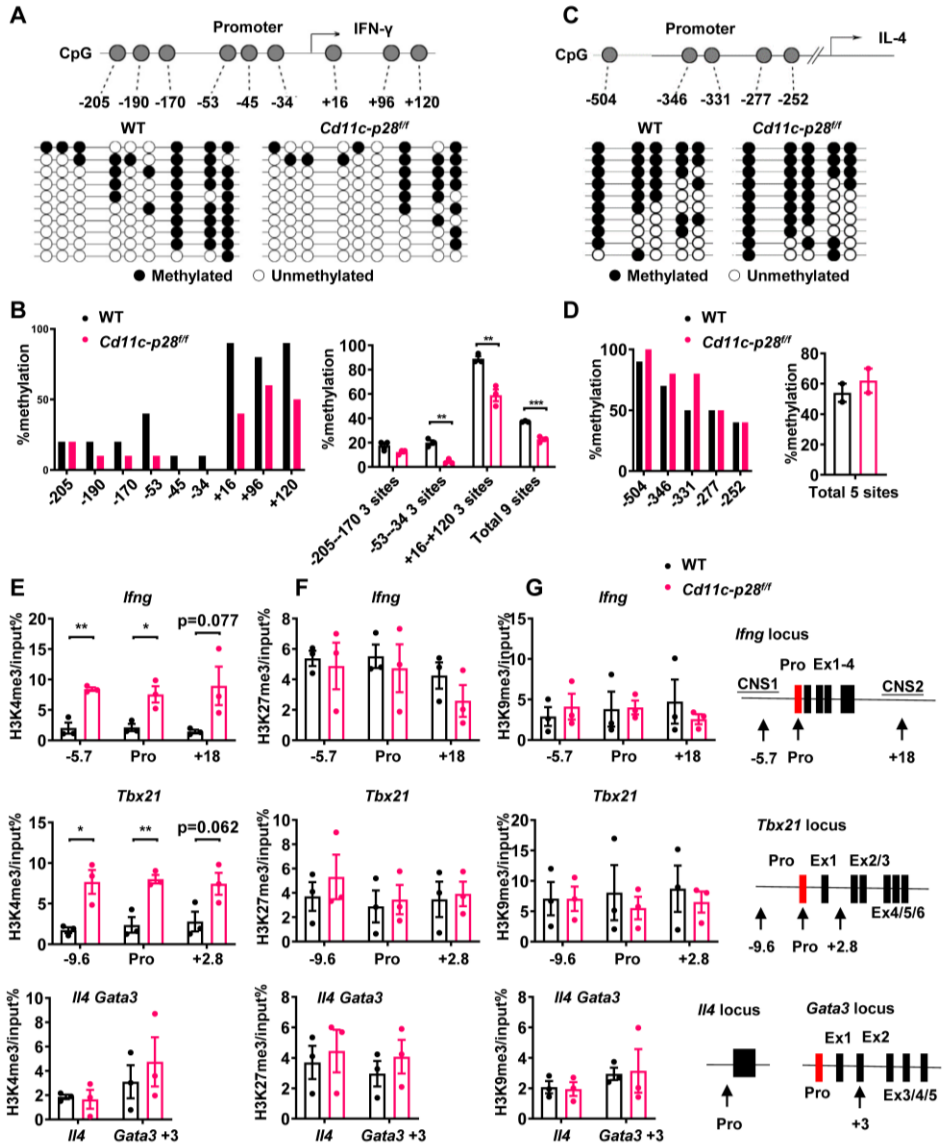

Figure 3. Distinct DNA and H3K4 methylation patterns at *Ifng* and *Tbx21* promoter regions in CD4SP thymocytes from *IL27p28*-deficient mice.

(A) DNA methylation analysis of nine CpG sites in the *Ifng* promoter using sodium bisulfite-treated genomic DNA from $GFP^{+}CD4^{+}CD8^{-}CD44^{lo}$ CD4SP thymocytes. Each row represents a sequenced allele (n=10 clones from one of the three independent experiments). Filled (●) and open (○) circles denote methylated and unmethylated cytosine, respectively.

(B) Left: Percent methylation at individual CpG sites from one representative

experiment. Right: Average methylation of three adjacent site groups (group1: -205, -190, -170; group2: -53, -45, -34; group3: +16, +96, +120) and all CpG sites (mean ± SD, n=3).

(C) DNA methylation analysis of five CpG sites upstream of the *Il4* transcription start site using sodium bisulfite-treated genomic DNA from $GFP^{+}CD4^{+}CD8^{-}CD44^{lo}$ CD4SP thymocytes. Each row represents a sequenced allele (n=10 clones from the two independent experiments). Filled (●) and open (○) circles denote methylated and unmethylated cytosine, respectively.

(D) Left: Graphs show the percentage of methylation at each individual site (left panel) or all CpG sites (right panel).

(E-G) Histone trimethylation analysis in freshly isolated CD4SP thymocytes from *IL27p28*-deficient and WT mice. ChIP-qPCR was performed using antibodies against H3K4me3 (E), H3K27me3 (F), and H3K9me3 (G). qPCR primers targeted promoter and trans-regulatory regions of *Ifng*, *Tbx21*, *Il4*, and *Gata3*. Data: mean ± SEM (n=3, duplicates). Significance: * $P<0.05$; ** $P<0.01$ (Student's *t*-test). Abbreviation: pro., promoter.

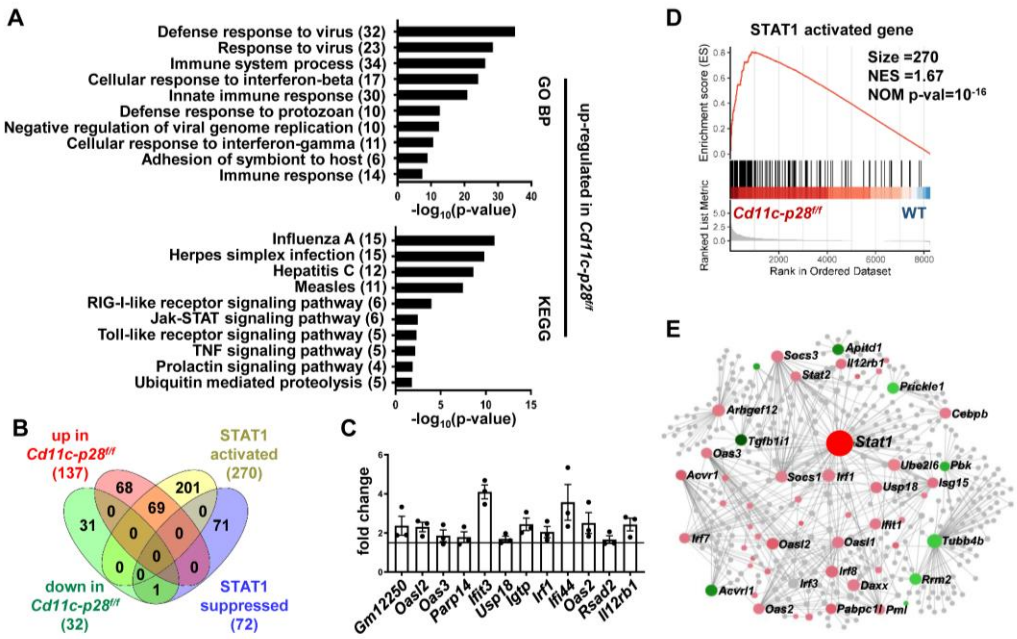

Figure 4. Increased expression of STAT1-activated genes in CD4SP thymocytes from *Cd11c-p28*$^{f/f}$ mice.

RNA-seq was performed to analyze the transcriptome of CD4SP thymocytes from *Cd11c-p28*$^{f/f}$and WT mice.

(A) Top 10 enriched Gene Ontology (GO) biological process and Kyoto Encyclopedia of Genes and Genomes (KEGG) pathways for up-regulated differentially expressed genes (DEGs) in *Cd11c-p28*$^{f/f}$ mice.

(B) Overlap between DEGs in *Cd11c-p28*$^{f/f}$ mice and STAT1-activated and suppressed genes. Numbers indicate overlapping genes in each category.

(C) Validation of RNA-Seq results by qPCR for representative up-regulated genes. Data: fold change in *Cd11c-p28*$^{f/f}$ versus WT mice (mean ± SEM, n=3, duplicates).

(D) Gene Set Enrichment Analysis (GSEA) showing coordinated upregulation of STAT1-activated genes in *Cd11c-p28*$^{f/f}$ CD4SP thymocytes.

884 (E) Protein-protein interaction network of DEGs. Nodes represent proteins; edges
885 indicate interactions. Larger nodes denote higher interaction degrees. Red: up-regulated;
886 green: down-regulated; gray: non-DEGs connected to the network (added by Network
887 Analyst).
888

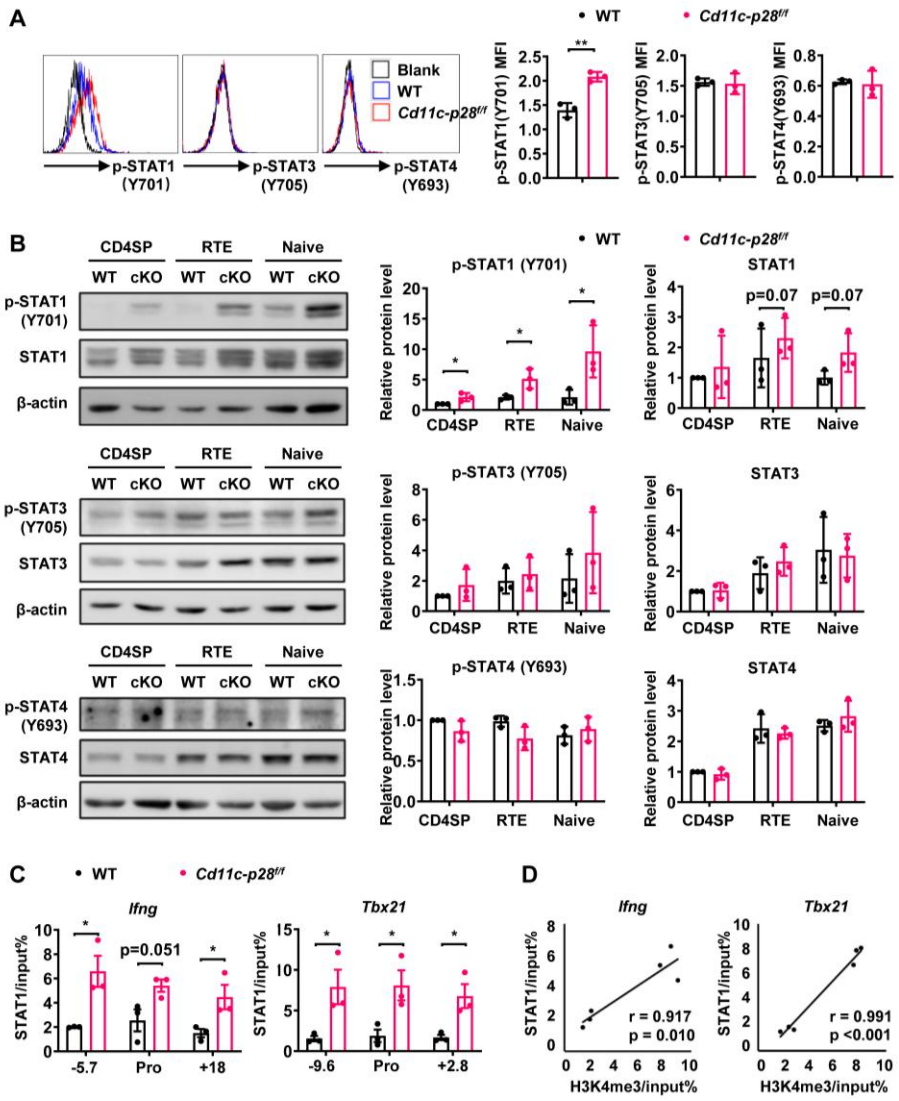

Figure 5. Enhanced STAT1 activation in CD4SP thymocytes from *Cd11c-p28*$^{f/f}$ mice. (A) Intracellular staining of freshly isolated thymocytes from *Cd11c-p28*$^{f/f}$ and WT mice using antibodies against phosphorylated STAT1 (Y701), STAT3 (Y705), and STAT4 (Y693). Representative histograms for CD4SP thymocytes (left) and mean fluorescence intensity (MFI) from three independent experiments (right, mean ± SD). (B) Western blot analysis of total and phosphorylated STAT1 (Y701), STAT3 (Y705), and STAT4 (Y693) in purified CD4SP thymocytes, CD4^{+} RTEs, and naive CD4^{+} T cells from *Cd11c-p28*$^{f/f}$ and WT mice. Representative blots (left) and relative protein levels quantified by densitometry and normalization to β-actin (right, mean ± SD, n=3).

(C) Increased STAT1 binding to promoter and regulatory regions of *Tbx21* and *Ifng* loci in *Cd11c-p28*$^{f/f}$ mice.

(D) Correlation between STAT1 binding and H3K4me3 levels at *Tbx21* and *Ifng* loci. Significance: * $P<0.05$; ** $P< 0.01$.

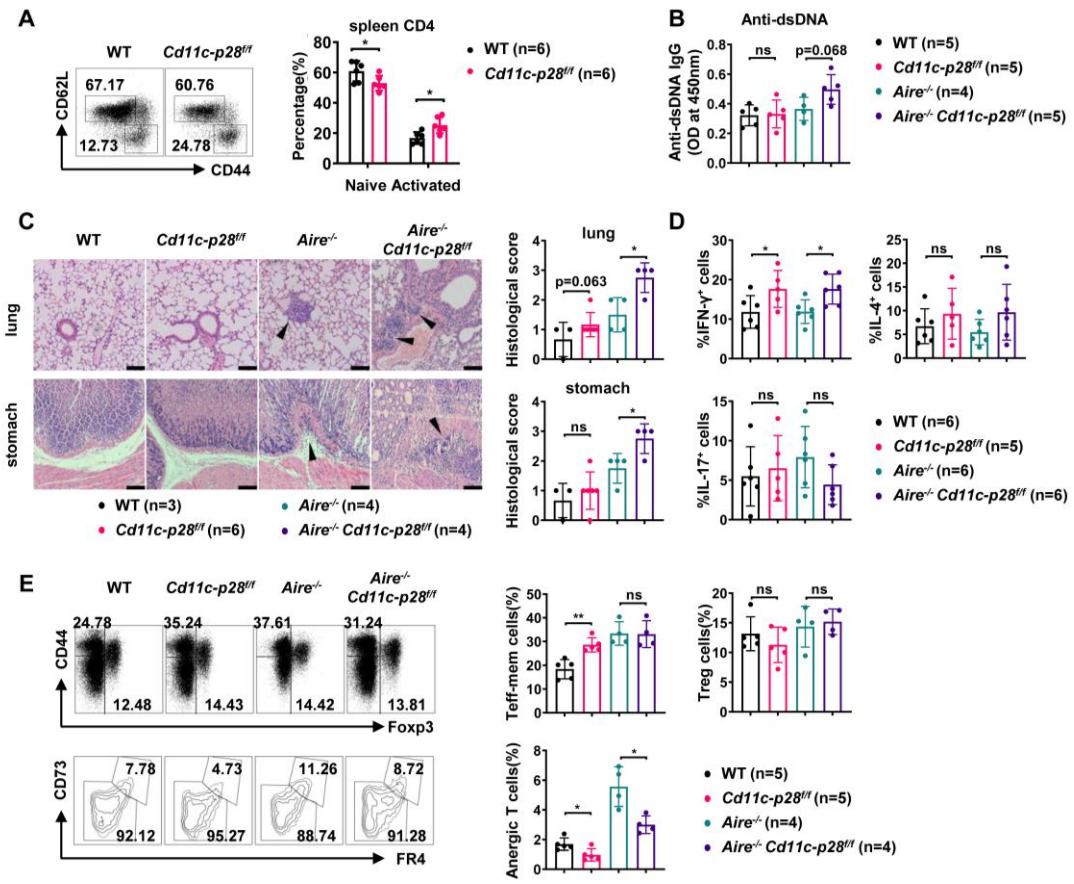

Figure 6. Exacerbated autoimmune responses in *Aire*$^{-/-}$ mice in the absence of IL27p28.

(A) CD44 and CD62L expression in CD4^{+} T cells from splenocytes of 6-8 week-old WT (n=6) and *Cd11c-p28*$^{f/f}$ (n=6) mice. Representative dot plots (left) and percentages of CD44^{lo}CD62L^{+} naive and CD44^{hi}CD62L^{-} activated T cells are shown (right, mean ± SD).

(B-D) WT, *Cd11c-p28*$^{f/f}$, *Aire*$^{-/-}$, and *Cd11c-p28*$^{f/f}$*Aire*$^{-/-}$ mice (24-30 weeks old) were analyzed. Each symbol represents one mouse (mean ± SD).

(B) Serum anti-dsDNA antibody levels (ELISA).

(C) H&E staining (left) and histological scores (right) of the lung and stomach. Arrows mark lymphocytic infiltrates. Scale bar = 100 μm.

(D) Percentages of IFN-γ^{+}, IL-4^{+}, and IL-17A^{+} CD4^{+} T cells in lung tissue after

PMA/ionomycin stimulation.

(E) Splenocytes from 12-week-old mice were stained for CD44, Foxp3, CD73, and FR4. Percentages of anergic ($CD4^{+}Foxp3^{-}CD44^{hi}CD73^{hi}FR4^{hi}$), effector/memory ($CD4^{+}Foxp3^{-}CD44^{hi}CD73^{lo}FR4^{lo}$), and regulatory ($CD4^{+}Foxp3^{+}$) T cells are shown. * $P<0.05$; ** $P<0.01$; ns, not significant.